EFFECTS OF EARTHQUAKE SOURCE PARAMETERS ON ESTIMATED GROUND MOTIONS

Yoshihiro NAKAO[1], Keiichi TAMURA[2] And Shojiro KATAOKA[3]

SUMMARY

The extremely strong ground motions in near-field from the 1995 Hyogoken Nanbu Earthquake caused serious damage to various kinds of structures. Recently semi-empirical methods have been noted as a synthesis technique to estimate ground motion including such strong ground motions in near-field. Though various earthquake source parameters have to be determined for the synthesis, it is very difficult to evaluate them with sufficient accuracy. In the present study, the effects of these parameters with expected variation on the estimated ground motions are evaluated for the application of the synthesis method to seismic design.

INTRODUCTION

In the early morning of January 17, 1995, the Hyogoken Nanbu(Kobe) Earthquake occurred causing serious damage to many kinds of structures. Although its magnitude was relatively moderate (Mj=7.2, Mj is Japan Meteorological Agency (JMA) Magnitude), extremely strong ground motions were generated. Its causative faults reached inland areas though the epicenter was located in the Akashi strait north of Awaji Island, which was unusual because most of the past large earthquakes in Japan were inter-plate earthquakes and therefor the causative faults were in the ocean areas. The destructiveness of the intra-plate inland earthquake was obviously ascribed to its extremely strong ground motions in near field, and records from the earthquake proved it. Many records show large peak acceleration and large response spectra. One of such records was obtained at Kobe Maritime Observatory of JMA (hereinafter described as JMA Kobe), whose peak acceleration was larger than 800 cm/sec^2 and the peak of the acceleration response spectra (damping ratio h=5%) of the horizontal components exceeded 2g.

Intra-plate inland earthquakes such as the Kobe Earthquake generate near field ground motions, which have different characteristics from those by inter-plate earthquakes in strengths and frequency characteristics. From the serious damage to many structures caused by extremely strong ground motions in the Kobe Earthquake, it was recognized that near field ground motion estimation techniques should be improved.

Recently semi-empirical method has been noted as an effective technique for synthesizing near field ground motions. Various earthquake source parameters such as fault length, width and dislocation rise time have to be determined for this synthesis. However, it is very difficult to determine these parameters with sufficient accuracy. Effects of source parameters with expected variation on the estimated ground motions should be evaluated when the technique is applied to seismic design[2]. In this paper earthquakes with the same magnitude as the Kobe Earthquake(Mj=7.2) are assumed to occur in the vicinity of the faults of the Kobe Earthquake and the ground motions at JMA Kobe from the earthquakes are synthesized using semi-empirical method. Source models with source parameters varied within expected range are used in the estimation and the extent of the synthesized ground motion variation is studied.

[1]   Earthquake Disaster Prevention Research Center, Public Works Research Institute, Japan, Email: nakao@pwri.go.jp
[2]   Earthquake Disaster Prevention Research Center, Public Works Research Institute, Japan, Email: tamura@pwri.go.jp
[3]   Earthquake Disaster Prevention Research Center, Public Works Research Institute, Japan, Email: s-katao@pwri.go.jp

EFFECTS OF VARIATION OF SOURCE PARAMETERS ON ESTIMATED GROUND MOTIONS

Ground Motion Synthesis Method Using Earthquake Source Model

In this paper ground motions are generated by a semi-empirical method[1]. In this method ground motion records from small events such as foreshocks and aftershocks with their hypocenters near the fault area of a large event are utilized as Green's functions to estimate a ground motion from a large event (Figure 1). The fault plane is divided into subfaults as large as the fault size of the small events. The Green's functions are summed up considering time delays due to fault ruptures from hypocenter to subfaults and wave traveling from each subfault to an estimation point. The Green's functions used in the semi-empirical method include complex effects of the dynamic rupture process on the fault, heterogeneous structures around the source and an estimation point. The semi-empirical method can be used to estimate ground motion component in wide period range including short period that is strongly affected by complicated underground structures on wave propagation path.
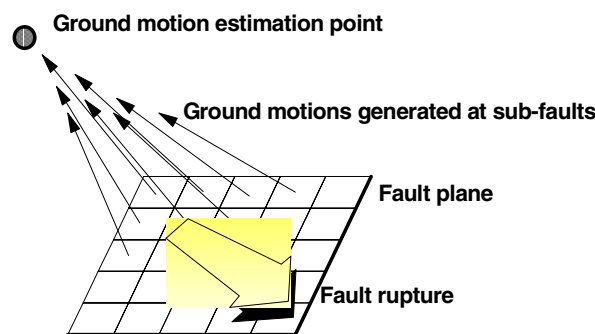

Fig. 1 Ground motion estimation

Target Ground Motion and Earthquake Source Parameters

In this paper the events with Mj=7.2 are assumed to occur in vicinity of the fault of the Kobe Earthquake. Ground motions at JMA Kobe from those events are synthesized. Basic earthquake source parameters such the location, strike and dip angle of the events are determined on the basis of the source model proposed by Kikuchi (1995) for the Kobe Earthquake[3], which are shown in Figure 2. Two fault locations are assumed and utilized as basic models so that effects of fault location on the estimated ground motions are evaluated.

Other source parameters such as fault length, width and dislocation for Mj=7.2 are deduced using the scaling law after Takemura[4]. The scaling law was proposed by regressing the source parameters for past Japanese intra-plate earthquakes. According to this scaling law, fault width is constant(13 km) for the events with $Mj \geq 6.8$. Rupture velocity and dislocation rise time are also determined by regressing the source parameters deduced for past intra-plate earthquakes[4]. Standard deviations calculated for the events with $Mj \geq 6.8$ are given to source parameters as expected variation ranges. Fig. 3 shows the relationship between magnitude(seismic moment) and earthquake source parameters which were deduced for the past earthquakes. Table 1 shows the source parameters determined for the assumed events with Mj=7.2 by the regression analysis and the standard deviations.
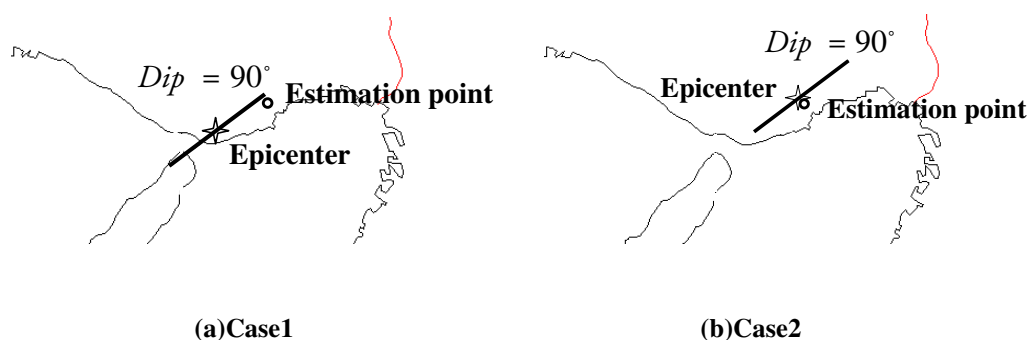

(a)Case1   **(b)Case2**

Fig. 2 Source Models for the ground motion synthesises

(a)Magnitude-Fault Length   **(b) Magnitude-Fault Width**   **(c)Magnitude-Dislocation**

(d) Seismic Moment- Rise Time   **(e)Seismic Moment-Rupture Velocity**
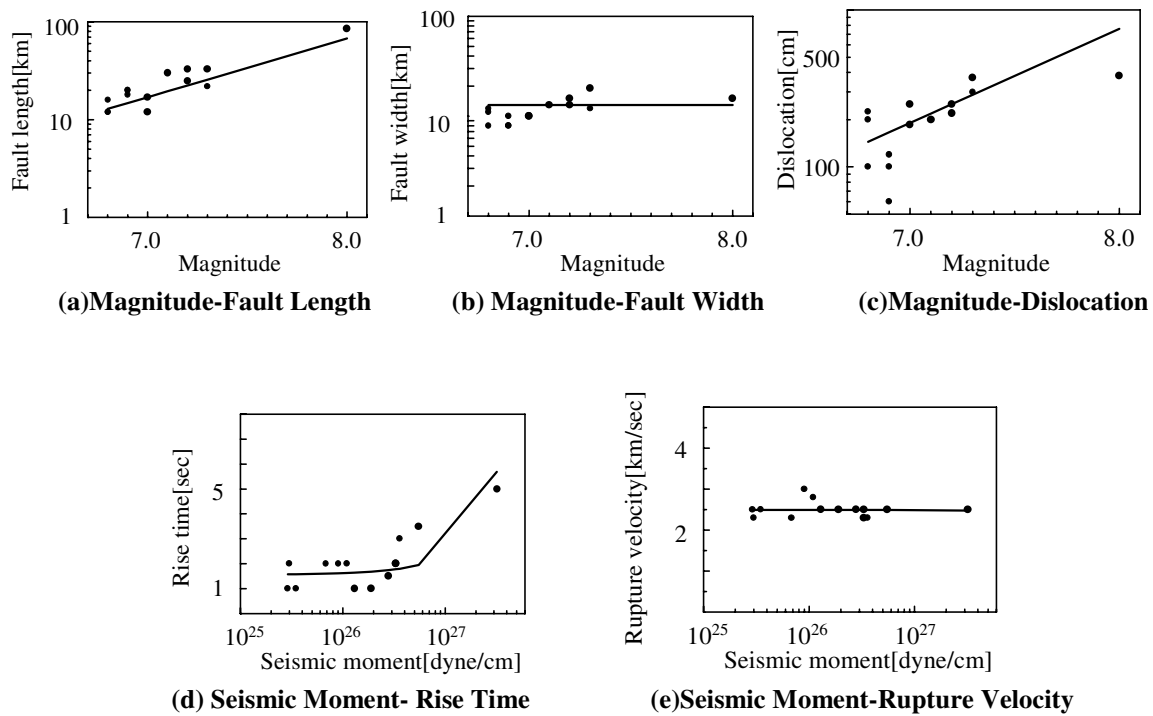**Fig. 3 Relationship between Magnitude(Seismic Moment) and Source Parameters**

Table 1 Source Parameters

Earthquake Source Parameter	Expected for Mj=7.2	Standard Deviation	
		+σ	-σ
Fault Length (km)	22.4	×1.29(28.9)	×1/1.29(17.4)
Fault Width (km)	13.0	+3.3(16.3)	-3.3(9.7)
Dislocation (m)	2.51	×1.52(3.82)	×1/1.52(1.65)
Rise Time (sec)	1.70	×1.48(2.52)	×1/1.48(1.15)
Rupture Velocity (km/s)	2.49	×1.08(2.69)	×1/1.08(2.31)

Ground motions are computed[1] with various source models shown in Table 2. As shown in Fig. 2 Case1 and Case2 are basic models with source parameters determined for an event with Mj=7.2 by regression analysis. The basic cases are different only in fault location. In Case1 the estimation point is located near the northern edge of the assumed fault while the observation point is near the center of the fault line on the ground surface in Case2. Cases1-2 to -23 and Cases2-2 to -23 are cases in which source parameters such as fault length, width, rise time, rupture velocity, hypocenter location, faulting process or distributions of asperities are varied in contrast with Case1-1 and Case2-1.

In contrast with Case1-1 and Case2-1 in which radial rupture process from fault center is assumed, the focus and the faulting process are varied in Cases1-10 to -17 and Cases2-10 to -17, respectively.

Cases1-18 to -23 and Cases2-18 to -23 are source models which add spatial variation of dislocation to Case1-1 and Case2-1, respectively. After Somerville et al. [5] the source models deduced for past earthquakes tend to have two asperities with 17.5% and 4.5% size of the total fault plane, on which dislocation is twice the average dislocation. In this paper an asperity whose size is 22% of total fault plane is assumed in order to specify the effect of asperity on the estimated ground motions. In Cases1-18 to -23 and Cases2-18 to -23 asperities shown in Fig. 4 are assumed.

Table 2 Analytical Cases

Model No.		Remarks
Case1	Case2	
Case1-1	Case2-1	Basic Case Uniform dislocation process are used in semi-empirical. Radial rupture extends from the fault center.
Case1-2	Case2-2	Variation of Case1-1 and Case2-1 in fault length by +σ.
Case1-3	Case2-3	Variation of Case1-1 and Case2-1 in fault length by -σ.
Case1-4	Case2-4	Variation of Case1-1 and Case2-1 in fault width by +σ.
Case1-5	Case2-5	Variation of Case1-1 and Case2-1 in fault width by -σ.
Case1-6	Case2-6	Variation of Case1-1 and Case2-1 in rise time by +σ.
Case1-7	Case2-7	Variation of Case1-1 and Case2-1 in rise time by -σ.
Case1-8	Case2-8	Variation of Case1-1 and Case2-1 in rupture velocity by +σ.
Case1-9	Case2-9	Variation of Case1-1 and Case2-1 in rupture velocity by -σ.
Case1-10	Case2-10	Variation of Case1-1 and Case2-1 in rupture process. Bilateral rupture extends from the fault center.
Case1-11	Case2-11	Variation of Case1-1 and Case2-1 in rupture process. Unilateral rupture extends from southwest.
Case1-12	Case2-12	Variation of Case1-1 and Case2-1 in rupture process. Unilateral rupture extends from northeast.
Case1-13	Case2-13	Variation of Case1-1 and Case2-1 in rupture start point. Radial rupture extends from central lower edge.
Case1-14	Case2-14	Variation of Case1-1 and Case2-1 in rupture start point. Radial rupture extends from southwestern central edge.
Case1-15	Case2-15	Variation of Case1-1 and Case2-1 in rupture start point. Radial rupture extends from southwestern lower corner.
Case1-16	Case2-16	Variation of Case1-1 and Case2-1 in rupture start point. Radial rupture extends from northeastern central edge.
Case1-17	Case2-17	Variation of Case1-1 and Case2-1 in rupture start point. Radial rupture extends from northeastern lower corner.
Case1-18	Case2-18	Spatial variation of dislocation shown in Fig. 4(a) is given to Case1-1 and Case2-1.
Case1-19	Case2-19	Spatial variation of dislocation shown in Fig. 4(b) is given to Case1-1 and Case2-1.
Case1-20	Case2-20	Spatial variation of dislocation shown in Fig. 4(c) is given to Case1-1 and Case2-1.
Case1-21	Case2-21	Spatial variation of dislocation shown in Fig. 4(d) is given to Case1-1 and Case2-1.
Case1-22	Case2-22	Spatial variation of dislocation shown in Fig. 4(e) is given to Case1-1 and Case2-1.
Case1-23	Case2-23	Spatial variation of dislocation shown in Fig. 4(f) is given to Case1-1 and Case2-1.

Southeastern Side   **Northwestern Side**

(a)Case1-18 and Case2-18   **(b) Case1-19 and Case2-19**   **(c) Case1-20 and Case2-20**

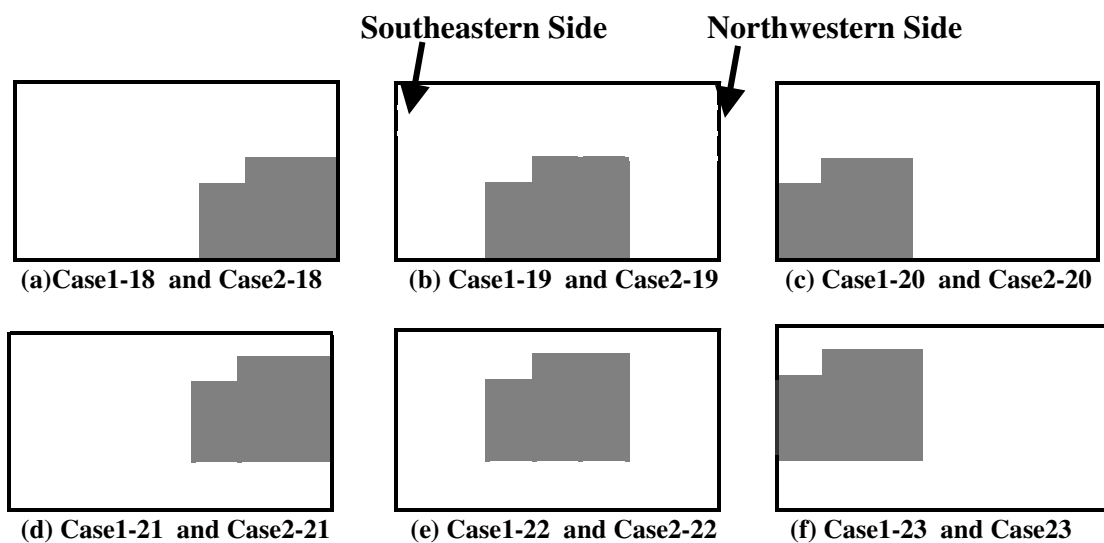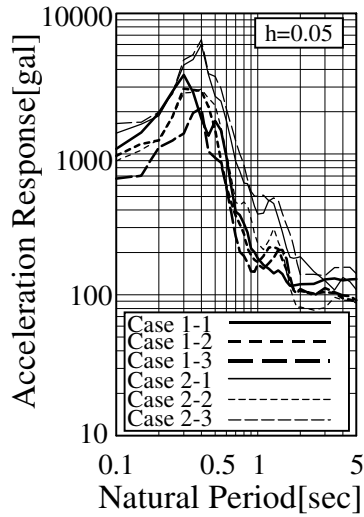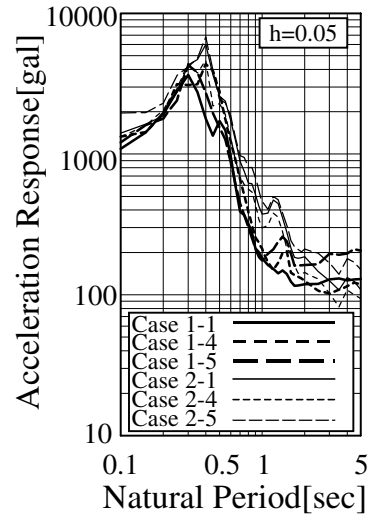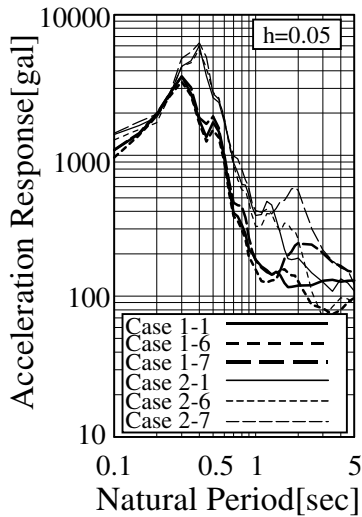**(d) Case1-21 and Case2-21**   **(e) Case1-22 and Case2-22**   **(f) Case1-23 and Case23**
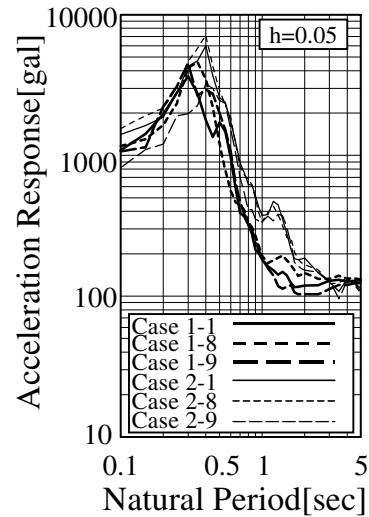**Fig. 4 Asperity distribution on fault plane**
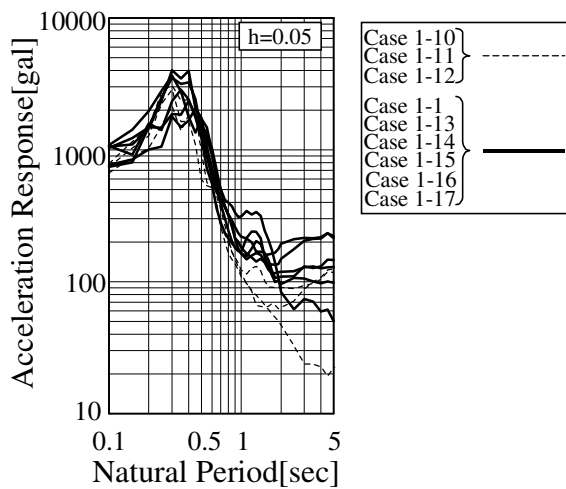
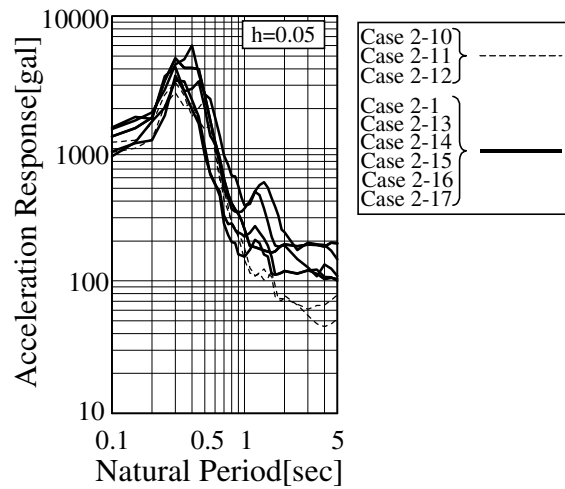**(a) Variation of fault length**

(b) Variation of fault width

(c) Variation of rise time

(d) Variation of rupture velocity

(e) Lateral and Radial rupture in Case 1 **(f) Lateral and Radial rupture in Case 2**
Figure 5 Variations of estimated ground motions due to variations of source parameters

Variation Parameter / Fault Location	(a) Fault Length	(b) Fault Width
Case 1	(a)-1 Log(Sa$_{+\sigma}$/Sa), Log(Sa$_{-\sigma}$/Sa)	(b)-1 Log(Sa$_{+\sigma}$/Sa), Log(Sa$_{-\sigma}$/Sa)
Case 2	(a)-2 Log(Sa$_{+\sigma}$/Sa), Log(Sa$_{-\sigma}$/Sa)	(b)-2 Log(Sa$_{+\sigma}$/Sa), Log(Sa$_{-\sigma}$/Sa)

Variation Parameter / Fault Location	(c) Rise Time	(d) Rupture Velocity
Case 1	(c)-1 Log(Sa$_{+\sigma}$/Sa), Log(Sa$_{-\sigma}$/Sa)	(d)-1 Log(Sa$_{+\sigma}$/Sa), Log(Sa$_{-\sigma}$/Sa)
Case 2	(c)-2 Log(Sa$_{+\sigma}$/Sa), Log(Sa$_{-\sigma}$/Sa)	(d)-2 Log(Sa$_{+\sigma}$/Sa), Log(Sa$_{-\sigma}$/Sa)

Spatial Variation of / Fault Location	(e)-S Sa$_{Upper}$ — Sa — Sa$_{Lower}$	(e)-C Sa$_{Upper}$ — Sa — Sa$_{Lower}$	(e)-N Sa$_{Upper}$ — Sa — Sa$_{Lower}$
Case 1	(e)-S-1 Log(Sa$_{Lower}$/Sa), Log(Sa$_{Upper}$/Sa)	(e)-C-1 Log(Sa$_{Lower}$/Sa), Log(Sa$_{Upper}$/Sa)	(e)-N-1 Log(Sa$_{Lower}$/Sa), Log(Sa$_{Upper}$/Sa)
Case 2	(e)-S-2 Log(Sa$_{Lower}$/Sa), Log(Sa$_{Upper}$/Sa)	(e)-C-2 Log(Sa$_{Lower}$/Sa), Log(Sa$_{Upper}$/Sa)	(e)-N-2 Log(Sa$_{Lower}$/Sa), Log(Sa$_{Upper}$/Sa)

Estimation point, Epicenter

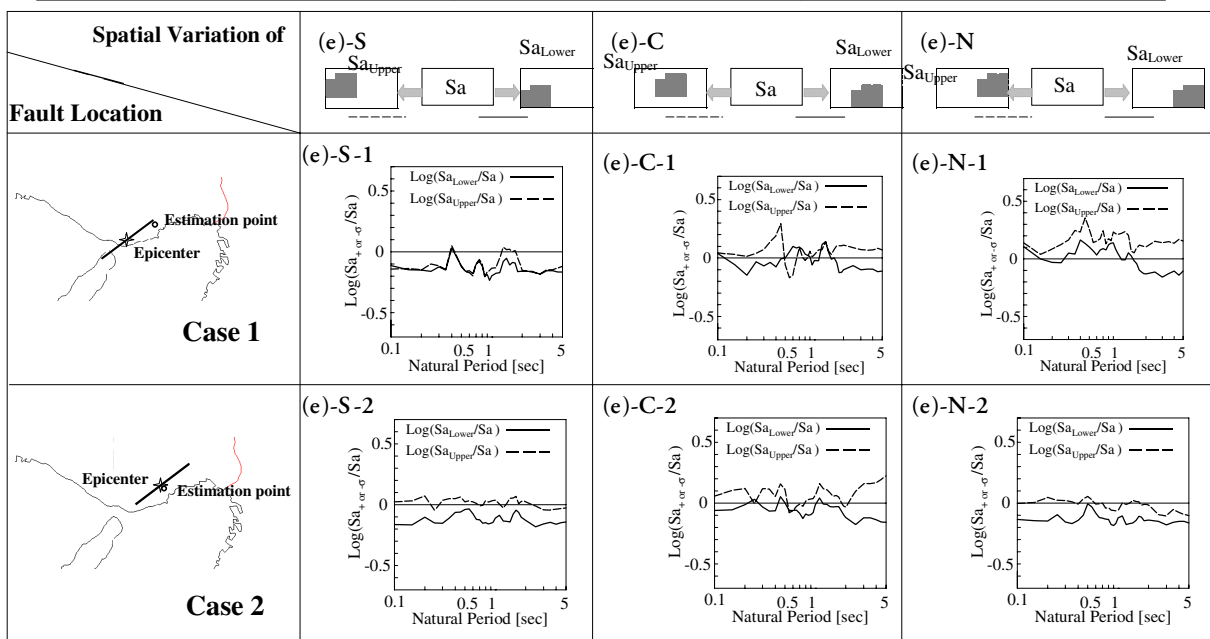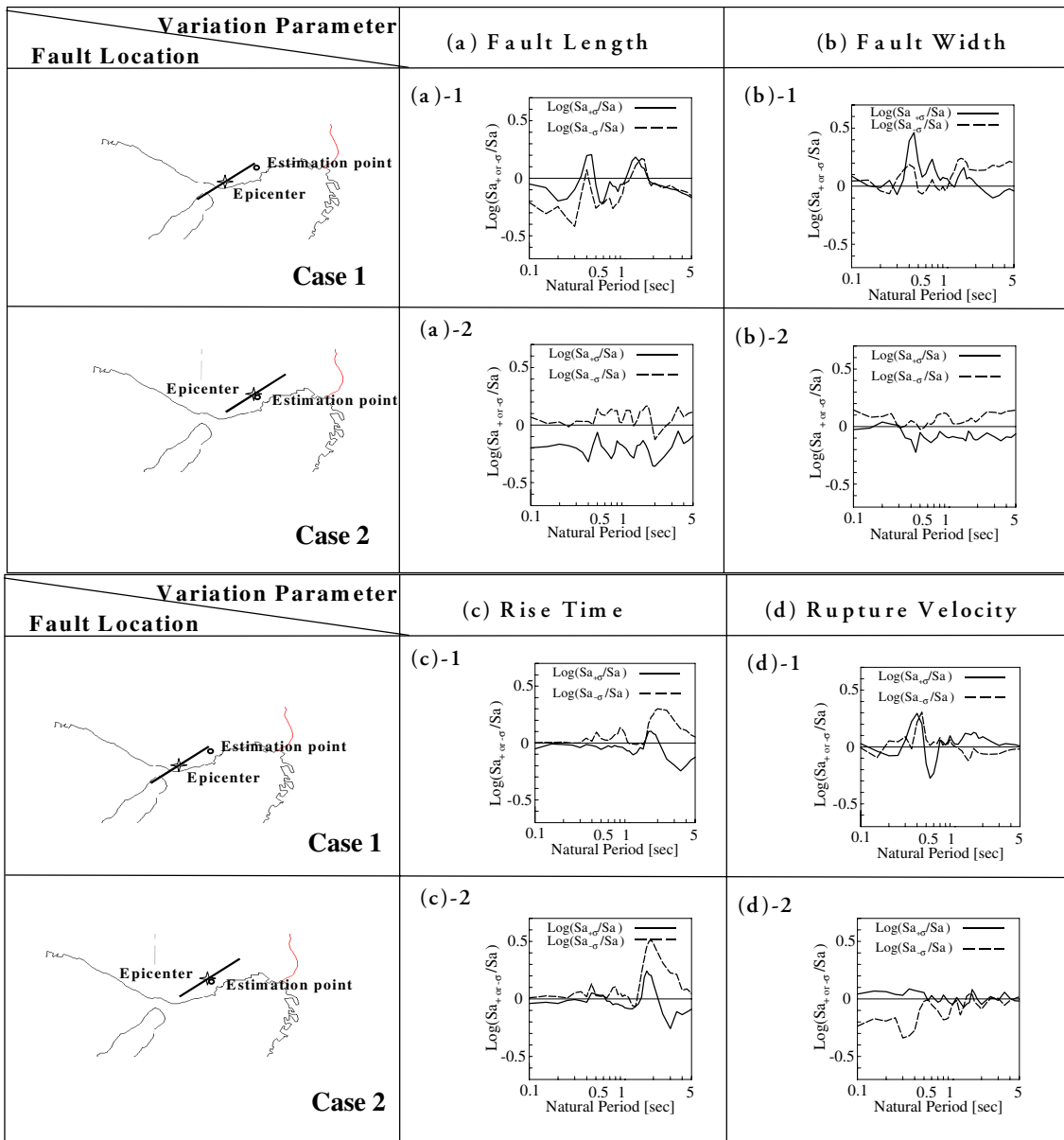Natural Period [sec], Log(Sa$_{+ \text{ or } -\sigma}$/Sa)

Figure 6 Spectral Ratio

6

Effects of Source Parameters on Estimated Ground Motion

An aftershock (Mj=5.2) ground motion of the Kobe Earthquake is used as a Green's function to synthesize ground motions from the assumed events in this paper. Figure 5 shows acceleration response spectra (damping ratio h=0.05) of estimated ground motions as the fault location and the source parameters such as fault length, width, rise time, rupture velocity, faulting process and spatial variation of dislocation are varied. To study the extent of estimated ground motion variation, Figure 6 presents the spectral ratio Rs defined by eq. (1) for each natural period.

$$Rs=Sa_{+\sigma}/Sa, \; Sa_{-\sigma}/Sa, \; Sa_{Upper}/Sa \; or \; Sa_{Lower}/Sa \qquad\qquad (1)$$

where $Sa_{+\sigma}$ and $Sa_{-\sigma}$ are the acceleration response values of ground motions generated from the faults with the source parameters increased and decreased by standard deviations, respectively, as shown in Table 1. Sa is acceleration response value of synthesized ground motion from the basic source model, i.e., Case1-1 or Case2-1. Sa_{Upper} and Sa_{Lower} are the acceleration response values of ground motions generated from the faults with the asperities on upper and lower part of the fault plane, respectively, as shown in Figures 6(e)-S, (e)-C and (e)-N.

For example, in Figures 6(a)-1 and 6(a)-2 solid and broken lines present the variations of estimated ground motions as the fault length determined for Mj=7.2 are increased and decreased by standard deviations, respectively. The fault location is assumed as Case1 and Case2 in Figures 6(a)-1 and 6(a)-2, respectively. Figures 6(b)-(d) present the cases in which fault width, rise time and rupture velocity are varied from the values determined for Mj=7.2 in Table 1.

In Figure 6(e) broken and solid lines represent estimated ground motion variations by distributing asperities on upper and lower part of the fault plane, respectively. Figure 6(e)-S, (e)-C and (e)-N are the cases in which asperities are placed on Southeastern, Central and Northwestern part of the fault plane. In Figures 6(e)-S-1, (e)-C-1 and (e)-N-1 fault location in the Case1 is assumed, and in Figures 6(e)-S-2, (e)-C-2 and (e)-N-2 fault location in the Case2 is assumed.

The effects of source parameters on estimated ground motions are summarized as follows.

(1)Fault Length, Width, Rise Time and Rupture Velocity

Figures 5(a)-(d) indicate that acceleration response values for Case2 are larger than those for Case1 in general.

In Figures 6(a)-1, 6(a)-2, 6(b)-1, 6(b)-2, 6(c)-1 and 6(c)-2 solid and broken lines have different values but they vary with natural period in similar way, which means in the case that the fault location is not changed, variations of fault length, width and rise time have similar influence on estimated ground motions. Furthermore, in Figures 6 (c)-1 and (c)-2 solid and broken lines vary with natural period in similar way even if the fault location is

changed from Case1 to Case2. The effect of rise time variation on the estimated ground motions does not depend much on the fault location as compared with the other source parameters such as fault length, width and rupture velocity.

Figures 6(a) and (b) show that in Case2 the spectral ratio does not vary with natural period as compared with the ratio in Case1. In Case2 fault length and width have approximately similar effects on estimated ground motion component at any natural period. Spectral ratio decreases as fault length and width are increased in Case2.

As rise time is increased, the spectral ratios in both Case1 and Case2 decrease in period range longer than 1.5 sec, while the ratio equals to almost 1 in the period range shorter than 1.3 sec. Variation of rise time has larger effect on the relatively long period component of estimated ground motions than short period component.Figure 6(d) shows that the variation of rupture velocity has larger effect on the estimated ground motions in short period range than long period range.

(2)Faulting Process

Figures 5(e) and (f) present the effect of faulting process on the estimated gound motions. In these figures broken lines show acceleration response spectra of ground motions estimated from faults with lateral rupture process. Other lines present response spectra calculated from the faults with radial rupture process. Lateral rupture tends

to generate weak ground motion component in the long period range as compared with radial rapture process. In Figures 5(e) and (f) the acceleration response values vary greatly in long period range. Variation of faulting process has larger effect on long period component of the estimated ground motions than short period.

(3)Spatial Variation of Dislocation

Figure 6(e) show that the spectral ratio in wide period range is greater than 1 in the case when the asperity is placed near the observation point and its depth is relatively shallow. The depth of asperity near the observation point has large effect on the estimated ground motion component in wide period range.

CONCLUSIONS

Ground motions were synthesized to study the effects of variation of earthquake source parameters on the estimated ground motions. The following conclusions are deduced from the present study.

1) As fault length, width and rise time are varied the spectral ratios are changed to different values but they vary with natural period in similar way. In the case that the fault location is not changed, variations of fault length, width and rise time have similar influence on estimated ground motions. Furthermore, as rise time are varied the spectral ratios vary with natural period in similar way even if the fault location is changed. The effect of rise time variation on the estimated ground motions does not depend much on the fault location as compared with the other source parameters such as fault length, width and rupture velocity.

2) Variation of faulting process has larger effect on long period component of the estimated ground motions than short period component.

3) The depth of asperities placed near the observation point has large effect on the ground motion component in wide period range.

ACKNOWLEDGMENTS

REFERENCES

[1] Irikura, K. (1986). "Prediction of Strong Acceleration Motions Using Empirical Green's Function", Proc. of 7th Japan Earthquake Engineering Symposium.
[2]Tamura, K. and Nakao, Y. "Strong Ground Motion Estimation Based on Source Modeling and Semi-empirical Green's Function Method", Proc. of the 14th U.S.-Japan Bridge Engineering Workshop
[3] Kikuchi, M. (1995). "Source Model For Kobe Earthquake", Chishitsu (Geology) News, Vol. 486 (in Japanese).
[4] Takemura, M. (1998)."Scaling Law for Japanese Intraplate Earthquakes in Special Relations to the Suface Faults and the Damages", Zishin, Vol. 51
[5] Somerville, P. G. et al.(1998). "A Study on Empirical Modeling of Slip Distribution on Faults", The 10th Earthquake Engineering Symposium
[6] Sato, R. ed. (1989). Japanese Source Parameters Handbook, Kajima Institute Publishing Co., Ltd. (in Japanese).